Fabrication of the (Y_2O_3: Yb-Er)/Bi_2S_3 Composite Film for Near-Infrared Photoresponse

Hong Jia[a], Ping Chen[a], Cheng Xu[a], Jiajia Zhou[b], Xiangwen Sang[a], Juechen Wang[a], Chang Liu[a], Xiaofeng Liu[a] and Jianrong Qiu[a.c]**

[a]*State Key Laboratory of Silicon Materials, School of Materials Science and Engineering, Zhejiang University, Hangzhou 310027, China*

[b]*College of Materials Science and Engineerging, China Jiliang University, Hangzhou 310018, China*

[c]*State Key Laboratory of Luminescent Materials and Devices, South China University of Technology, Guangzhou 510640, China*

Fax. & Tel.:+86-571-88925079; E-mail: qjr@zju.edu.cn and xfliu@zju.edu.cn.

1. Formation mechanism of the Y_2O_3: Yb-Er thin film.

Y_2O_3: Yb-Er thin films were prepared by a two-step process: formations of $M_2(OH)_{6-x}(NO_3)_x \cdot yH_2O$ (M = Y, Yb or Er, x=0-1), followed by an annealing process to achieve oxide films. The $M_2(OH)_{6-x}(NO_3)_x \cdot yH_2O$ was formed according to the following equations:

$$NO_3^- + H_2O + 2e \rightarrow NO_2 + 2OH^- \quad (1)$$

$$2Y^{3+} + (6-x)OH^- + xNO_3^- + yH_2O \rightarrow Y_2(\mathrm{OH})_{6-x}(\mathrm{NO_3})_x \cdot yH_2O \downarrow \quad (2)$$

$$2Yb^{3+} + (6-x)OH^- + xNO_3^- + yH_2O \rightarrow Yb_2(\mathrm{OH})_{6-x}(\mathrm{NO_3})_x \cdot yH_2O \downarrow \quad (3)$$

$$2Er^{3+} + (6-x)OH^- + xNO_3^- + yH_2O \rightarrow Er_2(\mathrm{OH})_{6-x}(\mathrm{NO_3})_x \cdot yH_2O \downarrow \quad (4)$$

Reduction of NO_3^- results in generation of OH^-, and causesan increase of pH value in the solution around the working electrode.Y^{3+}, Yb^{3+} and Er^{3+} precipitate with OH^- and NO_3^-, and a layer of $M_2(OH)_{6-x}(NO_3)_x \cdot yH_2O$ (M = Y, Yb or Er) forms on the working electrode, and then

Y_2O_3: Yb-Er film is achieved after annealing.

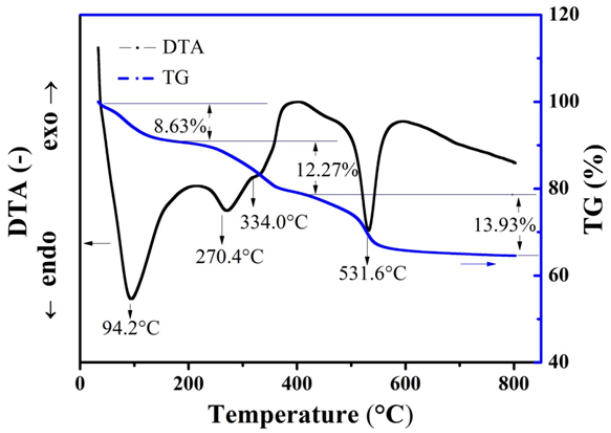

Figure S1.TG and DTA curves of $Y_2(OH)_{6-x}.(NO_3)_x \cdot yH_2O$ precursor

TG-DTA analysis.—The precursor ($Y_2(OH)_{6-x}(NO_3)_x \cdot yH_2O$) to be thermolyzed to Y_2O_3 during annealing was studied by TG–DTA. The thermal behavior of $Y_2(OH)_{6-x}(NO_3)_x \cdot yH_2O$ shows a multi-step process, as shown in figure S1. The decomposition of $Y_2(OH)_{6-x}(NO_3)_x \cdot yH_2O$ exhibited three steps in the TG curve, respectively. Endothermic peaks were observed at 94°C, 270~343°C, and 531°C, accompanied with three steps of weight losses, due to the following reactions:

$$Y_2(OH)_{6-x}(NO_3)_x \cdot yH_2O \xrightarrow{70-140^oC} Y_2(OH)_{6-x}(NO_3)_x + yH_2O\uparrow \quad (5)$$

$$Y_2(OH)_{6-x}(NO_3)_x \xrightarrow{270-340^oC} Y_2O_{(3-0.5x)}(NO_3)_x + (3-0.5x)H_2O\uparrow \quad (6)$$

$$Y_2O_{(3-0.5x)}(NO_3)_x \xrightarrow{400-580^oC} Y_2O_3 + xNO_2\uparrow + 0.5xO_2\uparrow \quad (7)$$

The first mass loss of 8.63% (calculated value for yH_2O, $y \approx 1.60$) at 94°C corresponds to the loss of the cointercalated water. The followed mass lose of 12.27% (calculated value for (6-x)OH, $x \approx 0.86$) is the result of decomposition of the yttrium hydroxide nitrate containing the hydrate water, which agrees well with the expected weight loss of 13.1%. When the OH group locating

at the different position of the yttrium hydroxide nitrate decomposes to water, the temperatures will be different (270°C and 343°C), but finally leaving a material of the "$Y_2O_{(3-0.5x)}NO_3)_x$". Complete decomposition of $Y_2O_{2.57}(NO_3)_{0.86}$ to Y_2O_3 occurs at 531°C with a further mass loss of 13.9%, which is in a good agreement to the theoretical weight loss of13.8%. No obvious mass loss was observed above 600°C.

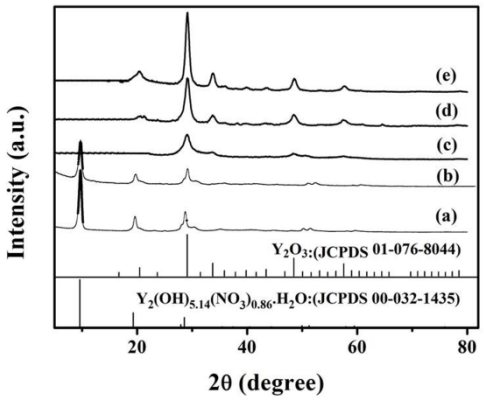

Figure S2. X-ray diffractions patterns of the samples before and after annealing at different temperatures: (a) Non-annealing, (b) 300 °C, (c) 400°C, (d) 500°C, and (e) 600°C.

2. XRD analysis

XRD patterns for samples (deposited from solution with Y:Yb:Er=96:3:1, mol%) beforeand after annealing are shown in figure S2. For the films without annealing and films annealed at 300°C, all the diffraction peaks ofthe samplescan be indexed as a pure $Y_2(OH)_{5.14}(NO_3)_{0.86}\cdot H_2O$ (JCPDS: 32-1435). The narrow peaks of the diffraction patterns indicate the good crystallinity of the samples.As shown in figure 2a and figure 2b, broader and weaker diffraction peaks were observed for the sample after annealing at 300 °C, indicating the low crystallinity of the sample after annealing at low temperature. After annealing at 400°C, 500°C and 600°C, the diffraction peaks assigned to $Y_2(OH)_{5.14}(NO_3)_{0.86}\cdot H_2O$ disappear, while new diffraction peaks emerge, which can be indexed as pure Y_2O_3 (JCPDS: 01-76-8044). The intensity of the diffraction peaks

increases while the full width at half maximum (FWHM) of the diffraction peaks decreases with increasing annealing temperature. This indicates that the crystallinity of the yttrium oxide films was enhanced when the annealing temperature increased from 400 ^{o}C to 600 ^{o}C.

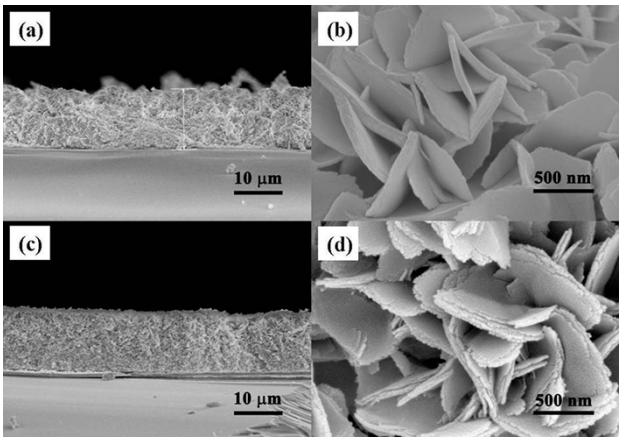

Figure S3. SEM images of the samples before and after annealing: (a) SEM image of the cross-section obtained from the as-prepared film, (b) SEM image of the as-prepared film, (c) SEM image of the cross-section obtained from a film annealed at 600 ^{o}C for 2.5 h, (d) SEM image of the film annealed at 600 ^{o}C for 2.5 h.

3. **SEM analysis**.

SEM images of the samples before and after annealing are presented in figure S3. Figure S3a and S3b are the cross-section and surface image of the Y_2O_3: 3%Yb-1%Er thin film without annealing. The film shows a flaky-like surface morphology, and the thickness of the film is about 12.6 μm. Figure S3c and S3d is the cross-section andsurface SEM images of the Y_2O_3: 3%Yb-1%Er thin film after annealing at 600^{o}C for 2.5 h. The film shows similar flaky-like surface morphology, and the thickness of the film is about 13.4 μm. The sheet shape of the annealed film decomposes to multi-layers structure, which may be ascribed to that the $Y_2(OH)_{5.14}(NO_3)_{0.86}$ turns into Y_2O_3 releasing gases of H_2O, NO_2 and O_2 during annealing.

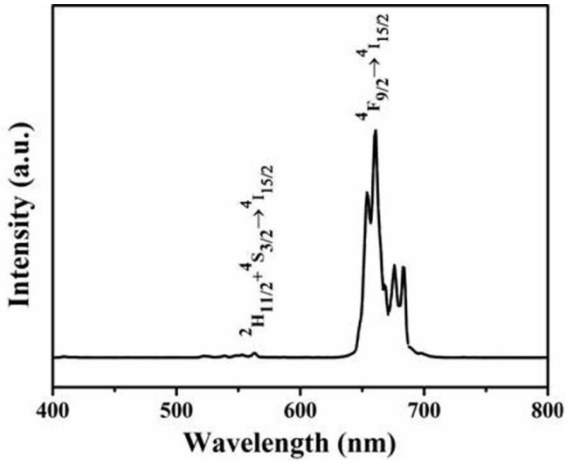

Figure S4. Up-conversion luminescence emission spectra from the film (Y_2O_3: 3%Yb-1%Er) after annealing at 600 ^oC for 2.5 h under 980 nm LD excitation.

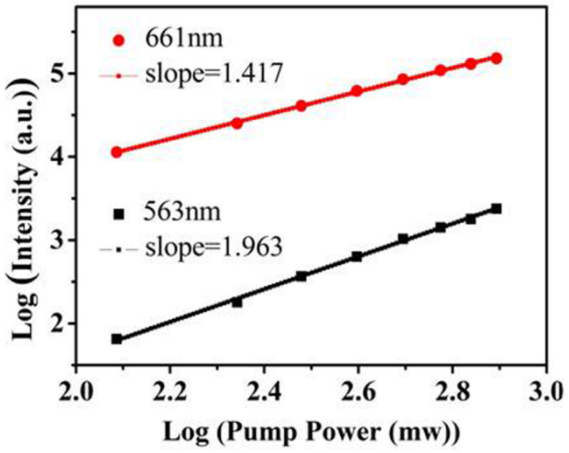

Figure S5. Power dependence of UC intensity of Y_2O_3: Yb-Er thin film doped with 3%Yb-1%Er measured at 661 and 563 nm, respectively.

4. Up-conversion luminescence properties

When excited by 980 nm laser diode, visible up-conversion emission was observed from the film (Y_2O_3: 3%Yb-1%Er) annealed at 600 ^oC for 2.5 h (figure S4.). Green emission bands observed from 531 to 571 nm are associated with the $^2H_{11/2}+^4S_{3/2}\rightarrow^4I_{15/2}$ transitions, while red bands peaking at 661nm are associated with the $^4F_{9/2}\rightarrow^4I_{15/2}$ transition. To explain the mechanisms of the up-conversion emission, the dependence of UC intensities on excitation power was measured.

It is well known that the dependence of UC intensity on pump power is essential for identification of the UC mechanism. For any UC process, the relationship between the intensity (I) and the pump power (p) is approximately expressed as follow equation:

$$I \infty P^n \tag{8}$$

Where the number of pumping photons (n) required to exciting ions from the ground state to the emitting state can be determined from the slope of the photoluminescence (PL) versus the laser excitation power in a log-log plot. The dependence of UC luminescence intensity of phosphor Y_2O_3:3%Yb-1%Er thin film upon pump power is shown in figure 5. The double logarithmic plot of the measured intensity of emission at 563 nm and 661 nm versus the pump power yields two straight lines with slope of 1.963 and 1.417, respectively, corroborating the fact that two-photon UC phenomena are occurring.

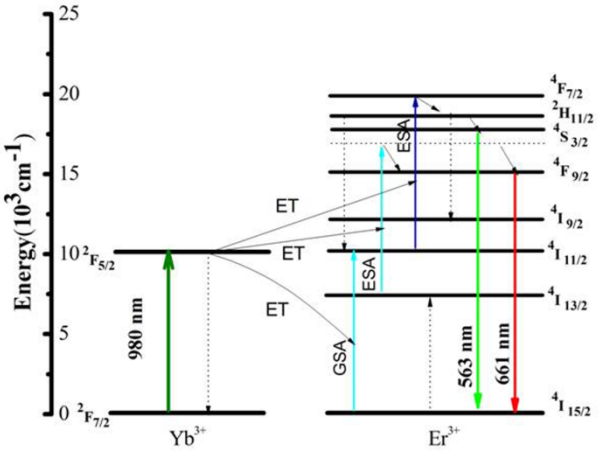

Figure S6. Proposed energy transfer mechanism under 980 nm LD excitation in the Y_2O_3: Yb-Er thin film (Y_2O_3: 3%Yb-1%Er).

As shown in figure S6, two main UC mechanisms may be used to explain the process of the red and the green up-conversion luminescence: the cascading nonradiative energy transfer from the Yb^{3+} to Er^{3+} ions and the multistep excited state absorption of Er^{3+} from another adjacent Er^{3+} ion. The Yb^{3+} ions possess a large absorption cross-section at 980 nm, and promote to its excited

state ($^2F_{5/2}$) then Yb^{3+} ion transfer its energy ($^2F_{5/2}\rightarrow{}^2F_{7/2}$) to an nearby Er^{3+} ion in its ground state promoting it to its $^4I_{11/2}$ excited state, or it transfers its energy ($^4I_{11/2}\rightarrow{}^4F_{7/4}$) to an Er^{3+} ion already in its $^4I_{11/2}$ excited state and promotes it to the $^4F_{7/2}$ excited state. Once the Er^{3+} ions are in $^4F_{7/2}$ excited state, multiphonon relaxations to the $^2H_{11/2}$+$^4S_{3/2}$ and $^4F_{9/2}$ states, then Er^{3+} ions lead to the green and red emissions from the $^2H_{11/2}$+$^4S_{3/2}$ and $^4F_{9/2}$ states, to the ground state. In the second case, 980 nm pumping photons excite Er^{3+} ion from its ground state ($^4I_{15/2}$) to the excited state ($^4I_{11/2}$), and subsequently, that ion absorbs the energy from an adjacent Er^{3+} ion in the same excited state ($^4I_{11/2}$), then reaching the $^4F_{7/2}$ excited state. The $^2H_{11/2}$+$^4S_{3/2}$ and $^4F_{9/2}$ states can be populated via multiphonon relaxations, and their radiative relaxation leads to the green and red emissions, respectively [1-3]. It is found that the red emission presents predominant emission, possibly, both energy transfer processes coexist. We have observed the red emission at 661 nm is the predominant one, and the green emission at 563 nm is relatively weak. Similar UC emission phenomena have been observed from the Yb and Er ions doped Y_2O_3 nanoparticles [4, 5].

In order to optimize the UC emission properties of the Y_2O_3: Yb-Er thin films, various experimental parameters which may affect the UC intensity of the Y_2O_3: Yb-Er thin films have been studied. The relationships between the UC intensity of theY_2O_3:Yb-Er thin film and various parameters are shown in figure S7. Figure 7a shows relations between the UC Intensity of the $^4F_{9/2}\rightarrow{}^4I_{15/2}$ transition with Yb^{3+} doping concentrations. Clearly, the UC luminescence property of the Y_2O_3: Yb-Er thin film strongly depends on the doping concentration of Yb^{3+}. The UC emission intensity reaches a maximum value when R (Yb/Er) is 3. A possible interpretation is proposed as follows. When the Yb^{3+} ion concentration increases from 1% to 3%, more Yb ions become available to furnish and transfer the energy to the Er^{3+} ions, resulting in the higher UC

emission intensity. If the Yb^{3+} ion concentration is further increased, the emission intensity decreases gradually, which may be ascribed to the cross-relaxation process for superfluous Yb ions. With the additional increase of the Yb^{3+} ions, the distance between neighboring Yb ions gets shorter, which can enhance the interaction of the neighbor Yb ions and the cross-relaxation process of Er ions, thus resulting in the concentration-dependent quenching. Thus, Y_2O_3: 3%Yb-1%Er thin film shows the strongest UC emission intensity. When the concentration of $Y^{3+}$was fixed at 96%, the UC intensity increases with increasing Yb^{3+}:Er^{3+} from 1%:3% to 3%:1%, and decreases with further increase to 3.5%:0.5%. The relations between the UC emission intensity of the $^4F_{9/2}\rightarrow{}^4I_{15/2}$ transition with the deposition time and the solution concentration are presented in figure 7c. The UC emission intensity increases with the extra deposition time from 1 to 20 minutes, and increases with increasing solution concentration from 0.01 to 0.1 M/L. It may be resulted from the increase in the thickness of the Y_2O_3: 3%Yb-1%Er thin film. Electro-deposition is closely related with the electron transfer process at the electrode surface,As deposition goes on, ITO substrate is gradually covered by the Y_2O_3:3%Yb-1%Er thin film. If the solution concentration is higher, ITO substrate will be covered faster. Figure 7d presents the relations between the UC emission intensity of the $^4F_{9/2}\rightarrow{}^4I_{15/2}$ transition with different annealing temperatures. The films without annealing or annealing at low temperature show similarweak UC emission intensity. The UC emission intensity increases with the annealing temperature from 400 to 600 ^oC, and then remains almost constant with further increasing annealing temperature. It is because the films without annealing and annealed at low temperature are mainly composed of $Y_2(OH)_{5.14}(NO_3)_{0.86}\cdot H_2O$. With increasing annealing temperature, the UC emission intensity of $^4F_{9/2}\rightarrow{}^4I_{15/2}$ transition increases dramatically due to the decomposition of $Y_2(OH)_{5.14}(NO_3)_{0.86}\cdot H_2O$ to Y_2O_3 with better crystallinity and low OH concentration which may

quench the UC luminescence through multiphonon relaxation.

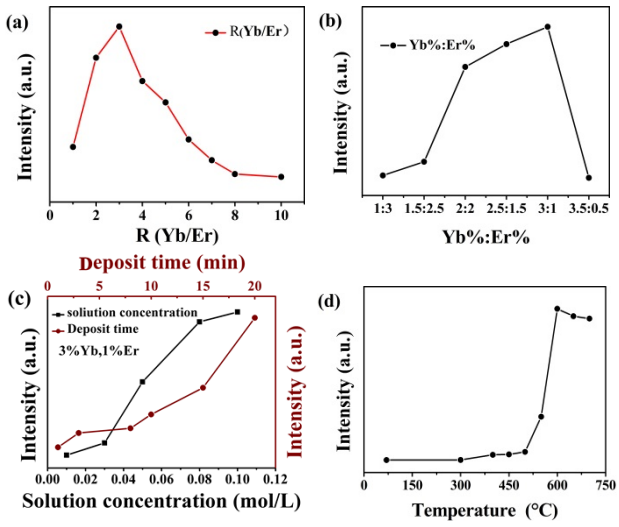

Figure S7. Relations between various preparation conditions and the red UC emission intensity of the Y_2O_3:Yb-Er thin films:(a) UC intensity of the $^4F_{9/2}\rightarrow{}^4I_{15/2}$ transitions as a function of R (R=Yb/Er), (b)UC intensity of the $^4F_{9/2}\rightarrow{}^4I_{15/2}$ transitions with doping concentration of Yb%: Er% (4%=Yb%+Er%), (c) Relations between UC intensity of the $^4F_{9/2}\rightarrow{}^4I_{15/2}$ transition of the Y_2O_3:3%Yb-1%Er thin film and the solution concentration as well as the deposition time,(d) Relation between UC intensity of the $^4F_{9/2}\rightarrow{}^4I_{15/2}$ transition of the Y_2O_3: 3%Yb-1%Er thin film with the annealing temperatures.

5. Photoelectrochemical measurements

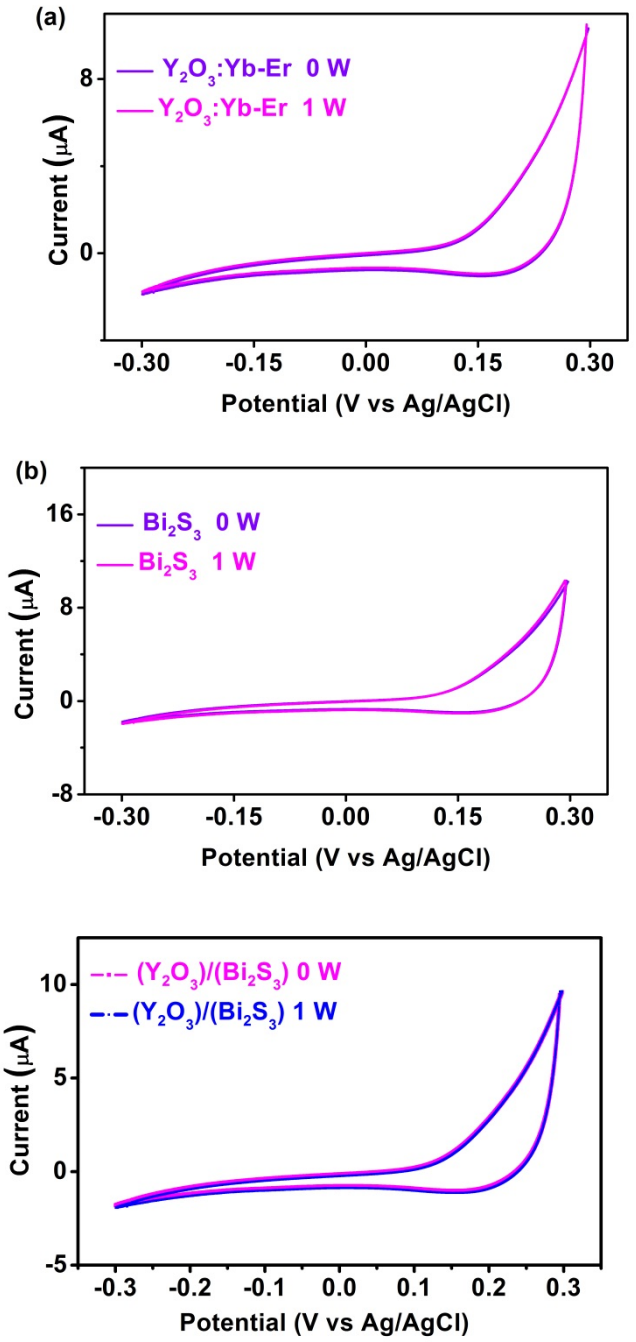

Figure S8. (a) Cyclic voltammetry potentiodynamic behaviors (i. e., I-V curves) of the Y_2O_3: Yb-Er film in the darkness(0 W) and excited by 980 nm laser diod at 1 W; (b) Cyclic voltammetry potentiodynamic behaviors (i. e., I-V curves) of Bi_2S_3 composite film in the darkness (0 W) and excited by 980 nm laser diod at 1 W; (c) Cyclic voltammetry

potentiodynamic behaviors (i. e., I-V curves) of $(Y_2O_3)/Bi_2S_3$ composite film in the darkness (0 W) and excited by 980 nm laser diod at at 1 W.

References

(1) Hirai, T.; Orikoshi, T. and Komasawa, I. *Chem. Mater.*, **2002**, *14*, 3576.
(2) MeZa, A.; Huerta, E.; Zaleta-Alejandre, E.; RiVeraz, Z. and Falcony, C. *J. Electrochem. Soc.*, **2013**, *2*, 2743.
(3) Oliva, J.; MeZa, O.; Diaz-Torres, L. A.; Salas, P.; Rose, E. D. L.; Martinez, A. and Angeles-Chavez, C. *J. Opt. Soc. Am. B.*, **2011**, *28*, 649.
(4) Huang, S. H.; Xu, J.; Zhang, Z. G.; Zhang, X.; Wang, L. Z.; Gai, S. L.; He, F.; Niu, N.; Zhang, M. L. and Yang, P. P. *J. Mater. Chem.*, **2012**, *22*, 16136.
(5) Jia, G.; You, H. P.; Song, Y. H.; Huang, Y. J.; Yang, M. and Zhang, H. J. *Inorg. Chem.*, **2010**, *49*, 7721.